Journal of the Electrochemical Society, Vol. 148, No. 9, 2001, pp. B348-B356.
ISSN: (Print 0013-4651) (Online 1945-7111)
DOI: 10.1149/1.1386626
http://www.electrochem.org/
http://scitation.aip.org/JES
http://www.ecsdl.org/getpdf/servlet/GetPDFServlet?filetype=pdf&id=JESOAN000148000000900B348000001&idtype=cvips&prog=normal

Electrochemical Behavior of Thin Film Analogs of Mg $(Zn,Cu,Al)_2$

T. Ramgopal, P. Schmutz, and G. S. Frankel
Fontana Corrosion Center, Department of Materials Science and Engineering, The Ohio State University

The electrochemical behavior of the intermetallic phase Mg(Zn, Cu, $Al)_2$ was studied using thin film compositional analogs prepared by flash evaporation. Characterization by scanning electron microscopy, atomic force microscopy, and Auger electron spectroscopy depth profiles indicated that the films were single phase, laterally homogenous, and homogeneous through the thickness. Experiments in deaerated 0.5 M NaCl showed that the addition of 18 atom % Cu to $MgZn_2$ raised the open circuit potential (OCP) by about 150 mV and the breakdown potential by 170 mV. The attack seemed to be localized dealloying. In high pH solutions where $Mg(OH)_2$ was stable, the films were susceptible to a more classical form of localized breakdown. The breakdown and the repassivation potentials increased with increasing copper concentration. Cyclic polarization curves on these films show the presence of Zn reduction peaks in the cathodic part of the downward potential scan. OCP playback experiments on the intermetallic thin films showed that the Mg(Zn, Cu, $Al)_2$ phase is very active over a wide range of compositions in neutral solutions at the OCP of the 7xxx series alloy.

The electrochemical behavior of the intermetallic compounds (IMCs) in aluminum alloys plays a crucial role in the localized corrosion process. Intermetallic compounds can be cathodic or anodic to the matrix of the alloy.[1] The electrochemical response of these intermetallic phases in an alloy is a function of composition, open circuit potential (OCP), and polarizability. Buchheit has compiled the OCP of various intermetallic particles in different environments, which is instructive in understanding the galvanic relations between the intermetallic particles and the matrix.[1] However, it is also important to know the electrochemical kinetics of each phase.

Cu-rich intermetallics have been investigated in recent years to understand their role in the localized corrosion of Cu-containing Al alloys. Studies on Al_7Cu_2Fe have shown that these particles are noble to the matrix of Al-Cu-Mg based alloys.[2] They have an OCP of —0.65 V *vs.* saturated calomel electrode (SCE) in 0.1 M NaCl.[2] These particles are polarized cathodically at the OCP of the alloy and the resulting high pH can cause trenching of the matrix around the particles. The θ ($CuAl_2$) phase particles are also noble to the matrix and can result in localized corrosion around the particles in Al-Cu alloys. θ phase has an OCP of —0.64 V SCE in deaerated 1 M NaCl. The OCP of the θ phase varies from —0.13 to —1.23 V SCE in Cl-free buffers over a range of pH[3]. The OCP of pure Al is below that of the θ phase over the entire range of pH, indicating that θ is noble to Al.[3] The Cu in the passive film on $CuAl_2$ was found to be metallic (Cu^0), which resulted in enhancement of the cathodic kinetics on this intermetallic phase.[3] The CuAl(Fe,Mn) phase present in AA2024 can be cathodic or dissolve locally exhibiting local anodes and cathodes within the heterogeneous particle.[4]

The S phase, $CuAl_2Mg$, plays a major role in the localized corrosion of AA2024.[5] The OCP of S phase in 0.5 M NaCl is —0.92 to —0.93 V SCE and is independent of aeration. The independence of OCP on aeration indicates that the anodic reaction on this phase is highly nonpolarizable.[5] Cyclic polarization curves on the S phase show that the zero current potential on the reverse scan is identical to the OCP prior to the scan, suggesting that there may be nonfaradaic liberation of Cu clusters from dealloyed $CuAl_2Mg$.[5] Rotating disk experiments also indicate that there is liberation of Cu from the intermetallic compound.[6] At the OCP of 2024, the S phase particles are under severe anodic polarization, which can result in dissolution of this phase. However, the dissolution of this phase may leave behind a Cu rich surface, which could be cathodic to the matrix.[5] It is also possible that during the dissolution process, there is nonfaradaic liberation of small Cu particles from a sponge-like remnant. Subsequent dissolution of such particles and redeposition of Cu on the Al alloy surface can result in redistribution of Cu to large distances on the surface of the alloy and the generation of large cathodic regions.[6]

High strength 2xxx and 7xxx series Al alloys are often very susceptible to localized corrosion in the presence of chloride. The localized corrosion can take the form of pitting, crevice, or inter-granular corrosion (IGC), including exfoliation. As pits or crevices grow, they often develop into IGC, which can grow deep into a structure. 7xxx aluminum alloys exhibit different corrosion behavior depending on the temper. The T6 peak-aged temper is more susceptible to IGC than the overaged T7 temper, and corrodes more in an EXCO test.[7] The T6 temper exhibits two breakdown potentials in potentiodynamic polarization experiments, whereas the T7 temper exhibits only one, suggesting a relationship with IGC susceptibility.[8,9] However, 24 h potentiostatic tests revealed IGC in both the T6 and T7 temper.[8] Analytical transmission electron microscopy (TEM) on grain boundary eta phase [$Mg(Zn, Cu, Al)_2$] showed that the particles in the T7 temper had much higher Cu concentration and lower Zn concentration than those in the T6 temper.[8] In order to understand the phenomenon of IGC in the 7xxx series alloys, it is important to characterize the electrochemical behavior of the grain boundary precipitate phases as a function of Cu, Zn, and Al concentration.

It has been reported that the intermetallic eta phase ($MgZn_2$), which is found in the 7xxx series alloys, is active to the Al alloy matrix, with an OCP of about — 1100mV SCE in 1 M NaCl.[10,11] However, the eta phase has considerable solid solubility for Cu as well as Al and there has been no systematic investigation of the electrochemical behavior of this phase as function of Cu and Al concentration. The aim of this work is to understand the electrochemical behavior of the eta phase over a range of composition and its role in IGC of the 7xxx series alloys.

Experimental

Thin film compositional analogs of intermetallic particles were prepared by flash evaporation. Flash evaporation is very similar to regular evaporation except that a device is used to feed powders onto a heated boat. The boat is hot enough to immediately evaporate (flash) all the powder.[12] As a result, there is no accumulation of powder in the boat, and the vapor flux has the stoichiometry of the powder fed into the boat.[12] Hence, films deposited by flash evaporation have a controllable stoichiometry and are uniform through the depth.[12]

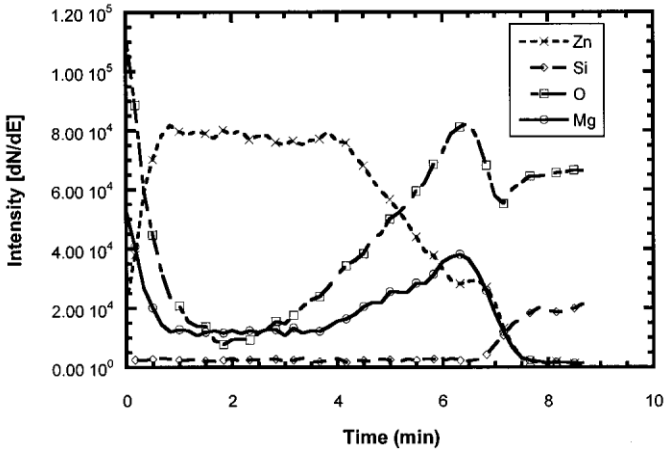

Figure 1. AES depth profile of an $MgZn_2$ thin film on oxidized Si.

For the deposition of Mg(Zn, Cu, Al)$_2$ (eta phase) thin films by flash evaporation, the starting material was alloy powder generated by crushing a cast ingot. Ingots of various compositions were cast by placing Mg, Zn, and Cu in an MgO crucible, which was inserted in a quartz tube. The quartz tube was then evacuated, backfilled with 0.25 atm of Ar and sealed. The encapsulated quartz tube was heated to 1150°C, held for 20 min, and furnace cooled to room temperature. The button obtained was multiphase, but overall had the desired composition. It was crushed into powder, which was used as the starting material for flash evaporation. Crushed alloy powder was preferred over mixed elemental powders because the crushed powder resulted in films of lower oxygen content. A dimpled Ta strip boat was used; no contamination by Ta in the films was observed. The average deposition rate was about 0.5 nm/s and the average thickness of the films was between 200 and 250 nm. The base pressure prior to evaporation was 2×10^{-7} Torr and the operating pressure was 8-10 $\times 10^{-7}$ Torr. It has been reported that Al thin films deposited with a base pressure of 2×10^{-7} Torr or better behave very similarly to the bulk material. Furthermore, the oxygen content for films deposited on Si substrates was found by energy dispersive spectroscopy (EDS) to be very low (about 1 atom %). Assuming that the influence of any structural differences is small, it is reasonable to expect that the behavior of these films would be representative of that of intermetallic particles of the same composition found in 7xxx series alloys.

Thin films were deposited on a number of different substrates, *e.g.*, Ta, MgO, Si with 300 nm of thermal oxide (SiO_2), and Si, in order to find the system that resulted in the lowest oxygen content in the metal deposit and best adhesion between the substrate and metal film. Si was chosen as the best substrate for deposition and subsequent electrochemical testing of the thin films because it provided good adhesion and the oxygen content in the films were low. The formation of a thin interfacial oxide layer promoted good adhesion between the Si substrate and film. Auger electron spectroscopy (AES) depth profiles used to characterize the composition of the thin films and scanning electron microscopy (SEM) micrographs show that the films are reasonably homogeneous, Fig. 1 and 2. The nominal composition of the thin films tested were Mg(Zn, Cu)$_2$, with overall Cu concentrations of 0, 4, 8, 18, and 27 atom % and Mg(Zn, Al)$_2$ with overall Al concentrations of 0, 4, and 10 atom %.

Electrochemical tests were carried out in deaerated 0.5 M NaCl (pH 7**)** and 0.5 M NaCl adjusted to pH 10.94 by NaOH additions. Tests were performed in high pH solution to determine

the effect of the stability of $Mg(OH)_2$ on the electrochemistry of the intermetallic thin films. Electrochemical tests were also performed in solutions containing 0.025 M Zn^{2+} to determine the effect of Zn ions on the breakdown potential. All electrochemical tests were performed at a scan rate of 5 mV/s, starting at the OCP with no initial delay.

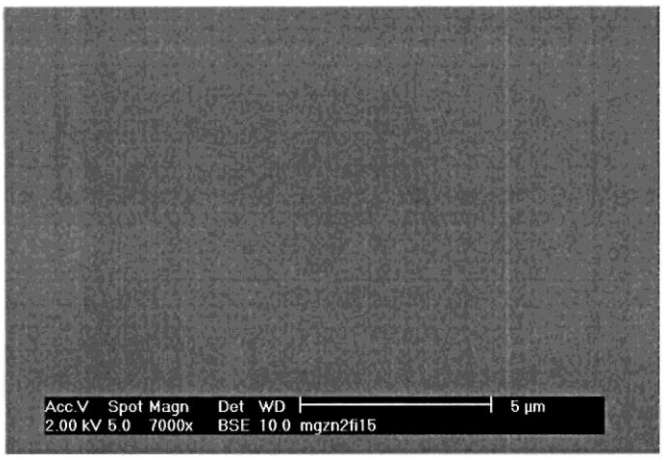

Figure 2. BSE SEM image of $MgZn_2$ thin film.

In order to investigate the electrochemical behavior of the IMCs when exposed as a component of an Al alloy, OCP playback experiments were performed on the thin film analogs of the grain boundary precipitates. The OCP of the 7150 alloy, in which $Mg(Zn, Cu, Al)_2$ IMCs are present, was measured and recorded as a function of time. In a separate experiment, the potential transient representing the OCP of 7150 was applied to the IMC thin film analog samples and the current responses of the thin films were measured as a function of the applied potential signal. OCP playback experiments were performed in both aerated and deaerated 0.5 M NaCl. All electrochemical measurements were run at least twice.

Results and Discussion

An AFM image of $MgZn_2$ is shown in Fig. 3; the topography of the film on a 1 µm scale is shown on the left and on the right is a Volta potential map of the surface determined by scanning probe force microscopy.[4] The films are relatively flat and have a surface roughness of about 5 nm. The Volta potential map shows no potential contrast in this region, indicating that the film is homogeneous. The value of the potential is —1400 mV *vs.* a Ni reference. This is in very good agreement with the potential measured in 0.5 M NaCl solution *vs.* an SCE reference electrode, both of which essentially indicate that $MgZn_2$ is very active. Backscattered electron images of thin films of all compositions also indicated that the films were homogeneous.

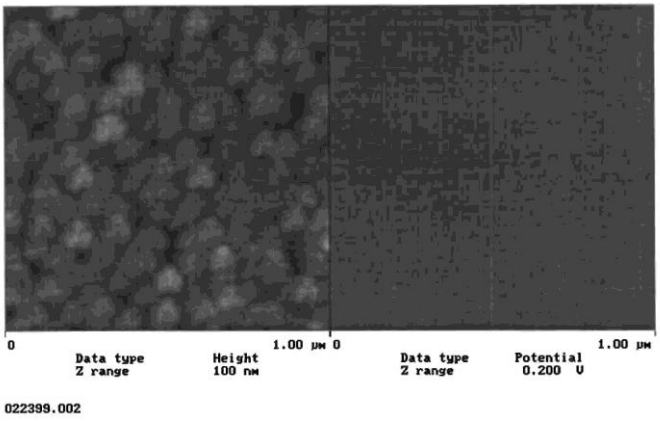

Figure 3. AFM image of $MgZn_2$ thin film, showing surface topography and Volta potential maps. The surface roughness is 5 nm and the Volta potential is —1400 mV *vs.* a Ni reference.

$MgZn_2$, $Mg(Zn, Cu)_2$, and $Mg(Zn, Al)_2$ in 0.5 M NaCl.—While the pH of the deaerated 0.5 M NaCl was not measured, it was assumed to be neutral and close to pH 7. The polarization curves for thin films of $Mg(Zn, Cu)_2$ containing 0, 4, and 8 atom % Cu in deaerated 0.5 M NaCl at a scan rate of 5 mV/s are given in Fig. 4. The OCP for $MgZn_2$ (0 atom % Cu) was −1400 mV SCE and a breakdown potential associated with a sharp increase in current was found at about −1140 mV SCE. A video system was used to observe the surface of the samples during the potentiodynamic polarization tests. No pits were observed on the surface of the sample. Corresponding to the sharp increase in current, dark regions initiated and grew rapidly. These observations may be associated with the dissolution of Zn. The reversible potential of Zn/Zn^{2+} is −1182 mV SCE, (assuming $[Zn^{2+}] = 10^{-6}$ M) which is very close to the measured breakdown potential of $MgZn_2$. Ignoring activity effects, the potential must be above the reversible potential of Zn in order to have any significant dissolution of Zn. It therefore seems reasonable that the breakdown potential is associated with the dissolution of Zn. This interpretation is supported by the large cathodic loop in the reverse scan with a maximum at about −1160 mV SCE. This loop results from a cathodic reaction that was not present during the forward scan. Since it is found near the reversible potential of Zn, and close to the breakdown potential on the forward scan, it likely results from back-plating of dissolved Zn ions generated by the dealloying process that occurred during the forward scan. Similar reduction/ oxidation peaks have been observed for Cu in copper based intermetallics like Al_2CuMg.

The reversible potential of Mg is very low and it dissolves at rapids rates in neutral chloride solutions. Hence, it is not unreasonable to expect that the high passive current density may be due to the dissolution of Mg.

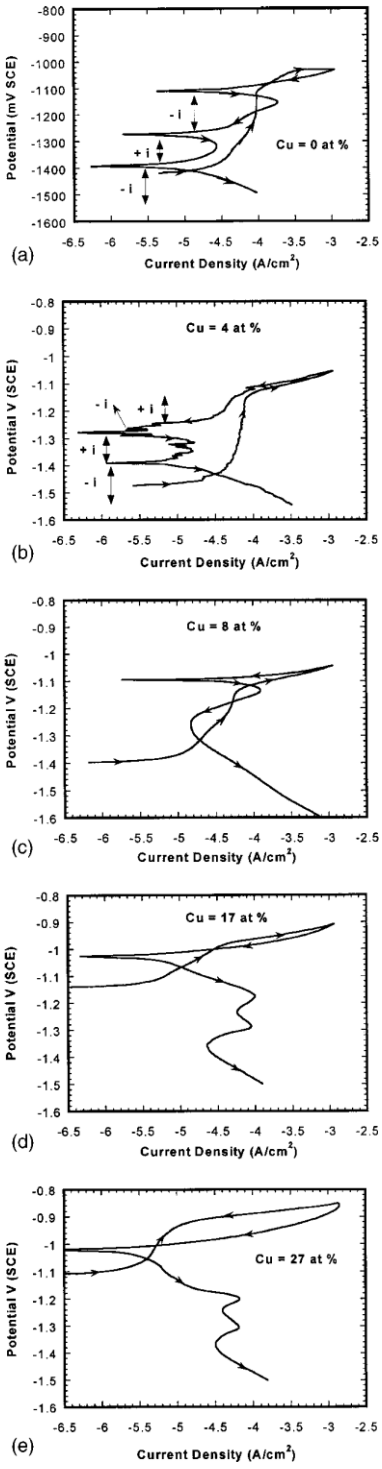

Figure 4. Polarization curve of $Mg(Zn, Cu)_2$ in deaerated 0.5 M NaCl (pH 7) at a scan rate of 5 mV/s. (a) Cu = 0 atom %, (b) Cu = 4 atom %, (c) Cu = 8 atom %, (d) Cu = 17 atom %, and (e) Cu = 27 atom %. Current polarity in the reverse scan is indicated on the graphs.

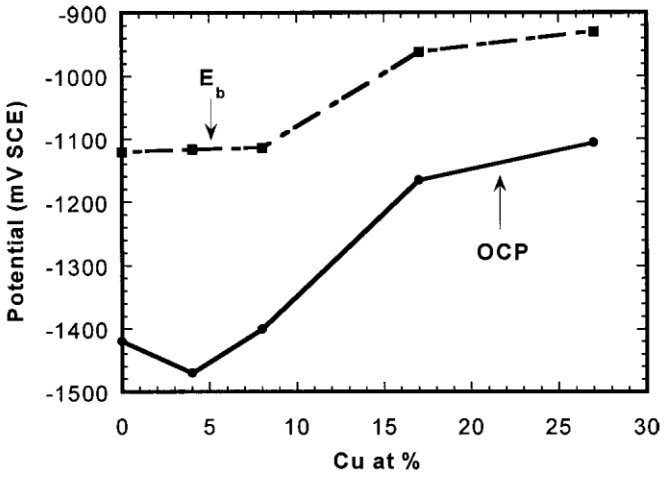

Figure 5. Variation in OCP and breakdown potential as a function of Cu concentration of $Mg(Zn, Cu)_2$ in deaerated 0.5 M NaCl.

The addition of 8 atom % Cu results in the OCP being slightly more positive than that for $MgZn_2$, although the OCP with the addition of 4 atom % Cu is a little lower than that of $MgZn_2$ (Fig. 4b). OCP values for passive metals can be highly variable because of the polarizability of the reaction, and the reasons for the effect of Cu on OCP are not clear. Copper additions up to about 8 atom % had a small influence on the breakdown potential. The breakdown of the films with 4 and 8 atom % Cu was similar to that described for 0 atom % Cu in that pitting was not observed. Rather, the breakdown appeared to be associated with Zn dissolution, which is supported by the visual observations as well as the presence of Zn reduction peaks on the reverse scans. As in the case of 0 atom % Cu, a cathodic loop is observed in the reverse scan for the sample with 4 atom % Cu. This cathodic loop is not clear in the polarization curve, but close inspection of the data shows that the current between −1250 and −1280 mV SCE is negative. The loop between −1280 and −1390 mV SCE is anodic. The reverse scan for the sample with 8 atom % does not contain a cathodic loop, but a large peak in the cathodic current is seen at about −1150 mV SCE. These features represent added cathodic current, which is likely associated with the redeposition of Zn back onto the electrode surface.

Samples with higher Cu concentrations (17 atom % and 27 atom %**)** exhibited polarization curves shifted considerably in the noble direction relative to $MgZn_2$ (Fig. 4d-e). The OCP was −1130 and −1100 mV SCE with the addition of 17 and 27 atom % Cu, respectively. The breakdown potential associated with dealloying was also shifted in the noble direction; −988 and −930 mV SCE for 17 and 27 atom % Cu, respectively, compared to about −1150 mV SCE for $MgZn_2$. The zero current potential during the downward scan is the same for the eta phase with 17 and 27 atom % Cu. The cyclic polarization curves for the thin films containing 17 and 27 atom % Cu show two peaks in the cathodic region of the reverse scan, at about −1200 and −1300 mV SCE, which are probably associated with reduction of Zn ions. The two peaks could indicate that Zn was present in different chemical states, or that there are two different sites onto which the Zn ions plate back.

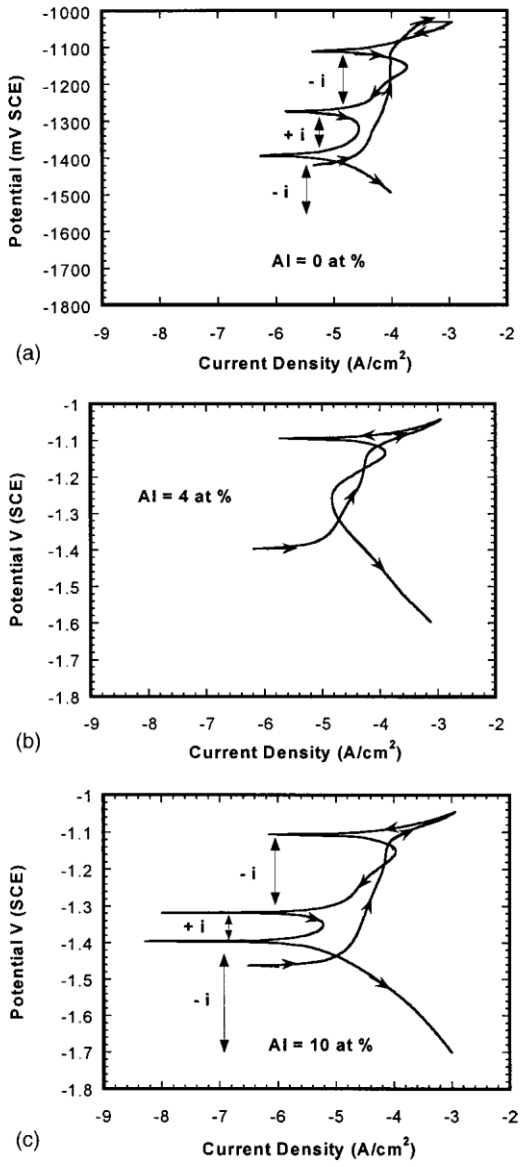

Figure 6. Polarization curve of $Mg(Zn, Al)_2$ in deaerated 0.5 M NaCl (pH 7**)** at a scan rate of 5 mV/s. **(**a**)** Al = 0 atom %, **(**b**)** Al = 4 atom %, and **(**c**)** Al = 10 atom %. Current polarity in the reverse scan is indicated on the graphs.

With increasing Cu concentration beyond 8 atom % (and correspondingly decreasing Zn concentration), the breakdown potential is ennobled, which suggests that the potential for Zn dissolution from the compound is a function of Zn or Cu content when the Cu content is high. Another interesting feature of the polarization curves is that the zero current potential on the reverse scan for all the copper containing alloys is higher than that of the original OCP, which is an indication of Cu enrichment on the surface of the electrode. This further supports the idea that the breakdown potential is associated with the dealloying of Zn from the alloy. Similar observations have been made for other Cu-bearing intermetallics like bulk T_1 (Al_2CuLi).[14] In the case of Al_2CuMg however, due to the nonfaradaic liberation of Cu, the OCP on the return scan is identical to the initial OCP.[5] The results of the OCP and the breakdown potential are summarized in Fig. 5.

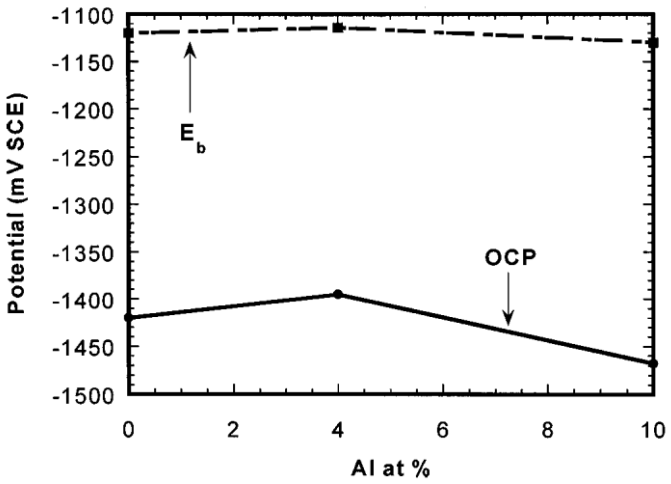

Figure 7. Variation in OCP and breakdown potential as a function of Al concentration of $Mg(Zn, Al)_2$ in deaerated 0.5 M NaCl.

The polarization behavior of the $Mg(Zn, Al)_2$ intermetallic thin films as a function of aluminum concentration is given in Fig. 6. Addition of up to 10 atom % Al does not alter the breakdown potentials associated with the dissolution of Zn. As for the case of $Mg(Zn, Cu)_2$, the first potential of zero current on the return scan is similar to the breakdown potentials on the forward scan and cathodic loops are found in the downward scan. For the same reasons as stated above, these cathodic loops are likely associated with plating of Zn ions from solution. The OCP and breakdown potential as a function of Al concentration is given in Fig. 7.

In order to understand the behavior of the IMCs in an alloy microstructure at the OCP of that alloy, OCP playback experiments were performed. First, the OCP of 7150 was recorded in deaerated 0.5 M NaCl. This alloy OCP as a function of time was then applied as the input signal to the potentiostat in a separate experiment on the intermetallic compound thin film sample, and the current response of the intermetallic compound was measured (Fig. 8, 9). The OCP of AA7150-T6 in deaerated 0.5 M NaCl increased with time from about −1220 mV SCE initially to −980 mV SCE at the end of 1 h. The OCP transient is shown in each of the figures along with the current transients measured on the thin film thin film IMC analogs during the OCP playback experiments. The intermetallic compounds with a low Cu concentration, *i.e.*, 4 and 8 atom %, were anodic for the entire transient and over the entire range of alloy OCP (Fig. 8b, c). These intermetallic compounds began dissolving rapidly during the OCP playback experiments at an applied potential of about −1090 to −1050 mV SCE, which is close to the breakdown potential of these compounds as measured during potentiodynamic polarization experiments. The peak current density for the 4 and 8 atom min % Cu was 400 and 800 $\mu A/cm^2$, respectively. The peaks in current density transients after 10-15 were associated with complete dissolution of the thin films. Since the thin films dissolved completely, the portions of the current transients after the current peak are not meaningful. However, the use of the thin films on the order of 200 nm in thickness is justified by the fact that the particles at the grain boundaries in 7xxx alloys are of this size or smaller, and complete dissolution of the particles should occur at similar potentials in similar time scales.

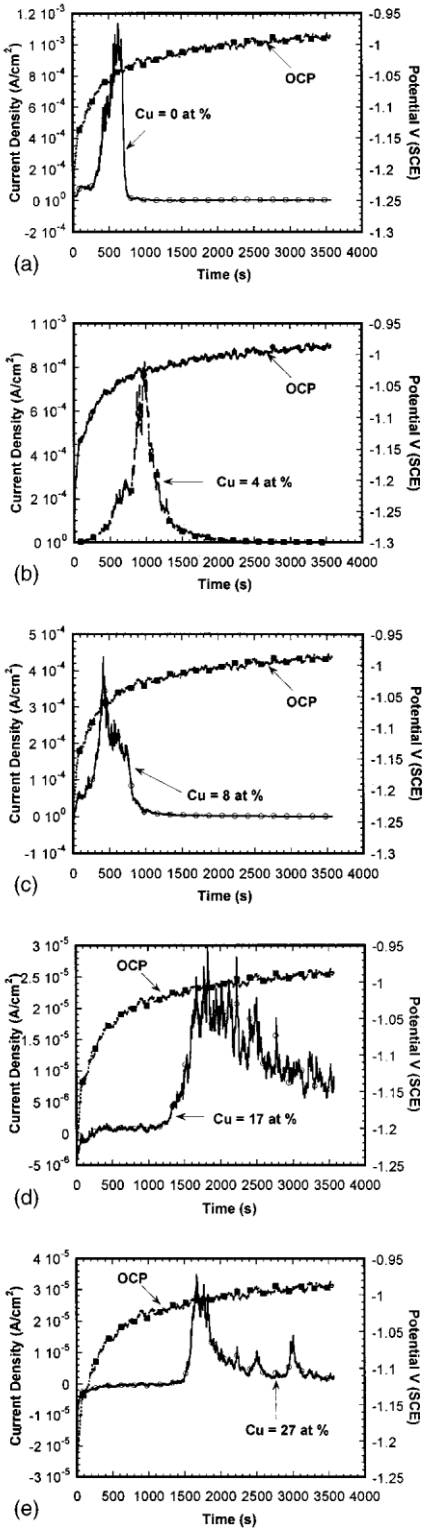

Figure 8. OCP playback experiments for $Mg(Zn, Cu)_2$ as a function of the OCP of 7150-T6 in deaerated 0.5 M NaCl. **(a)** Cu = 0 atom %, **(b)** Cu = 4 atom %, **(c)** Cu = 8 atom %, **(d)** Cu = 17 atom %, and **(e)** Cu = 27 atom %.

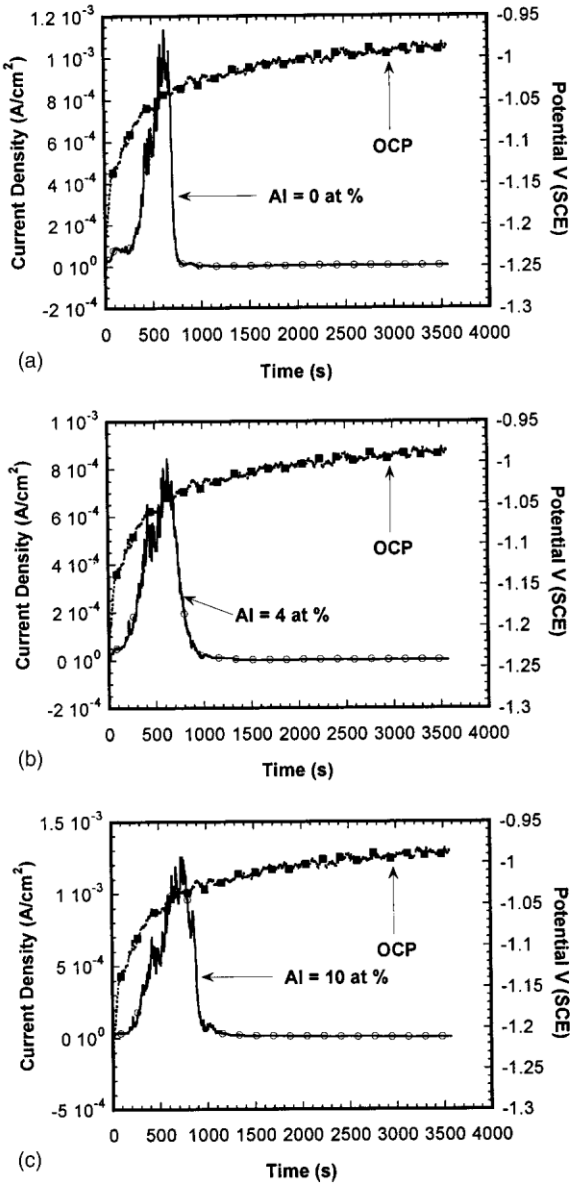

Figure 9. OCP playback experiments for $Mg(Zn, Al)_2$ as a function of the OCP of 7150-T6 in deaerated 0.5 M NaCl. (a) Al = 0 atom %, (b) Al = 4 atom %, and (c) Al = 10 atom %.

For higher Cu content films, the current density in the OCP playback experiment was initially cathodic at low applied potentials, and subsequently switched to anodic as the potential increased (Fig. 8d, e). The current densities in these cases were an order of magnitude lower than that observed for the low Cu content compounds indicating that the addition of 17 atom % Cu and above decreased the dissolution kinetics relative to the low Cu films. The 17 and 27 atom % Cu samples did not dissolve away during the OCP playback experiments, but the surfaces became enriched in Cu at the end of the experiment, as indicated by visual observation of the sample turning red as well as EDS measurements, which showed indicated that the Cu concentration was 35 and 45 atom % after the experiments on the 17 and 27 atom % Cu alloys, respectively. The OCP of 7150 remained near or below the breakdown potentials of these films

in the same solution (Fig. 8d, e).

These experiments suggest that the low Cu containing intermetallic compounds, when present in the 7xxx series alloy, will completely dissolve during exposure at OC in deaerated chloride solution. This might then stabilize localized attack. However, in the case of high Cu containing alloys, the particles are not completely dissolved at OC. These particles dealloy and may lead to the enrichment of Cu, which can affect the corrosion behavior of the 7xxx series alloy.

OCP playback experiments on $Mg(Zn, Al)_2$ intermetallic thin films showed that, for up to 10 atom % addition of Al, the intermetallic thin films completely dissolved rapidly after about 10 min at the alloy OCP (Fig. 9). The current density response as a function of time is similar to that of $MgZn_2$, which is consistent with the potentiodynamic polarization behavior of the intermetallic thin films as a function of Al concentration.

The OCP in aerated chloride solutions for many aluminum alloys is pinned at the pitting potential, accompanied by spontaneous pitting. OCP playback experiments were performed in aerated 0.5 M NaCl in order to understand the role of the intermetallic compounds in the localized corrosion behavior of the 7xxx series alloys (Fig. 10). $Mg(Zn, Cu)_2$ intermetallic thin films over the entire range of Cu concentration dissolved actively with peak current densities in the range of 10 to 1 mA/cm^2 (Fig. 10). $Mg(Zn, Al)_2$ thin films also dissolved rapidly for all Al concentrations (Fig. 11), with peak current densities in the 10 mA/cm^2 range. The thin film samples dissolved completely within 30-60 s of exposure to the alloy OCP, regardless of composition.

The effect of Zn^{2+} in solution on the breakdown potential of $Mg(Zn, Al)_2$ is shown in Fig. 12 and 13. It was found that when the Zn^{2+} concentration was increased from 0 to 0.025 M, the breakdown potential was raised from -1130mV to -1074 mV SCE. (In the case of the 0.025 M Zn^{2+}, the OCP is pinned at the breakdown potential.) This increase in breakdown potential with increasing Zn^{2+} concentration in solution supports the notion that the breakdown potential is indeed associated with dissolution of Zn from the thin film analogs. Increasing concentration of Zn^{2+} ions in solution would cause the reversible potential of Zn to increase and hence would shift the breakdown potential associated with Zn dissolution.

$MgZn_2$, $Mg(Zn,Cu)_2$, and $Mg(Zn,Al)_2$ in 0.5 M NaCl (pH 10.94).—The oxide film on the as-deposited surface of the intermetallic thin films is Mg rich, as shown by the AES depth profile in Fig. 1. Under conditions where this Mg oxide layer is stable, the thin films are susceptible to a more standard pitting type of attack associated with localized breakdown of the passive film. The Pourbaix diagram of Mg shows that $Mg(OH)_2$ is stable at high pH. Hence, in high pH[15] solutions and in the presence of aggressive chloride ions, the intermetallic thin films are expected to be susceptible to pitting. Figure 14 shows the behavior of the eta phase with varying copper additions at pH 11. Video observation confirmed that pits were formed above the breakdown potential. EDS analysis indicated that the corrosion product or pit remnant was enriched in copper by a factor of almost 2.

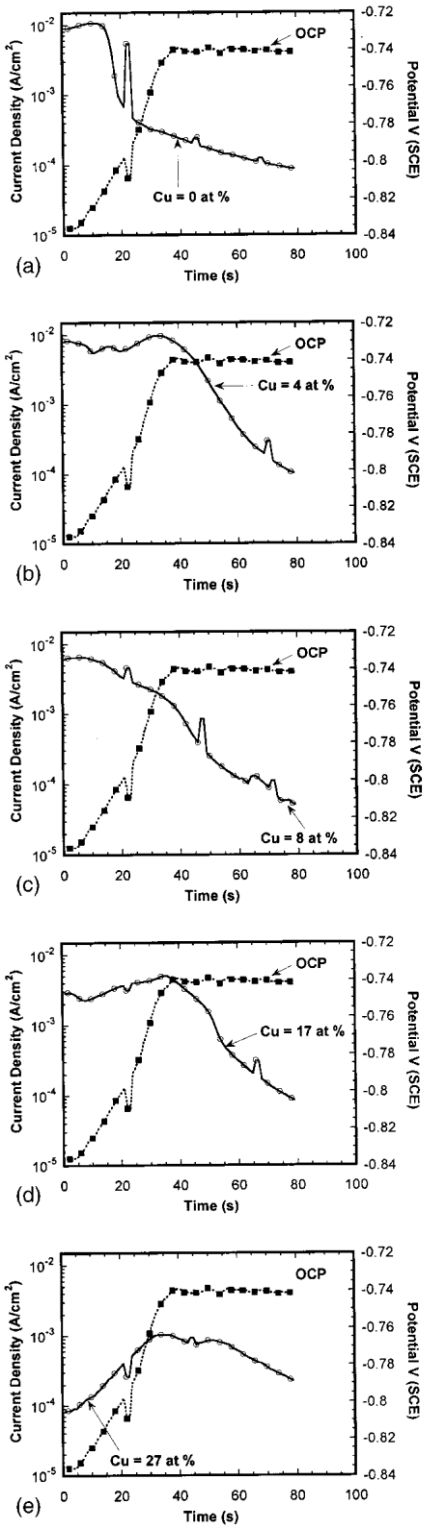

Figure 10. OCP playback experiments for $Mg(Zn, Cu)_2$ as a function of the OCP of 7150-T6 in aerated 0.5 M NaCl. **(**a**)** Cu = 0 atom %, **(**b**)** Cu = 4 atom %, **(**c**)** Cu = 8 atom %, **(**d**)** Cu = 17 atom %, and **(**e**)** Cu = 27 atom %.

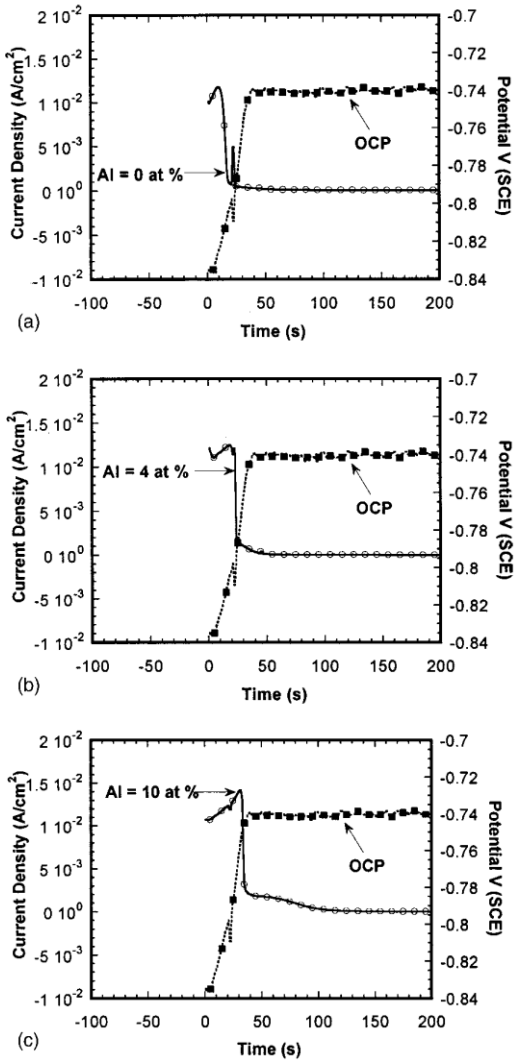

Figure 11. OCP playback experiments for $Mg(Zn, Al)_2$ as a function of the OCP of 7150-T6 in aerated 0.5 M NaCl. **(**a**)** Al = 0 atom %, **(**b**)** Al = 4 atom %, and **(**c**)** Al = 10 atom %.

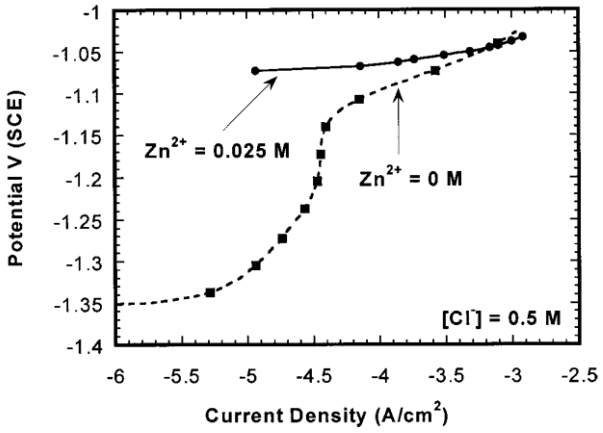

Figure 12. Effect of Zn^{2+} concentration on polarization curves for $Mg(Zn, Al)_2$, Al = 4 atom %.

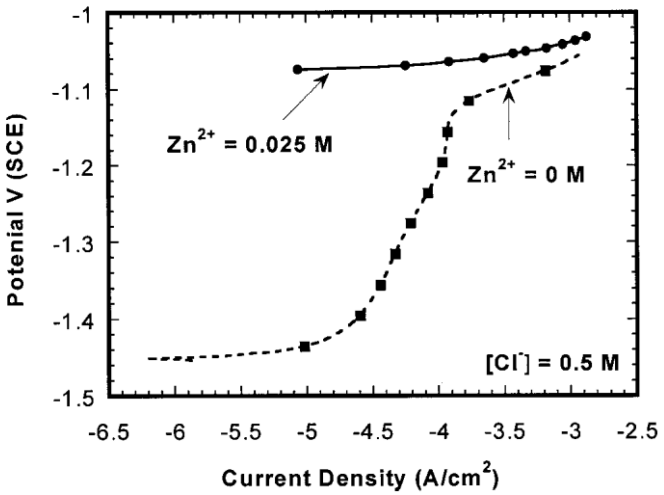

Figure 13. Effect of Zn^{2+} concentration on polarization curves for $Mg(Zn, Al)_2$, Al = 10 atom %.

The results of electrochemical testing in neutral and high pH environments suggest that dealloying and Cu enrichment occur in both cases. Enrichment of Cu on the electrode surface was observed in neutral pH environment when polarized to potentials above the breakdown potential. However, unlike the case of high pH environments, no localized breakdown (*i.e.*, pits on the electrode surface) was observed and the attack was more uniform in nature. In the high pH environment, there was localized breakdown due to the enhanced stability of $Mg(OH)_2$, and subsequent dealloying at the active pit wall. The dissolution in the "pits" was associated with localized dealloying of Zn and Mg resulting in the enrichment of Cu. Similar results have been reported in binary aluminum alloy thin films where the corrosion product was enriched in the noble element.

The polarization behavior of the $Mg(Zn, Cu)_2$ as a function of Cu concentration in 0.5 M NaCl (pH 10.94) is shown in Fig. 14. The passive current density decreased with increasing copper concentration. Addition of 4 atom % Cu has a small influence on the breakdown and repassivation potentials. In fact, the breakdown potential with 0 atom % Cu is slightly higher than for 4 atom % Cu, but is within the experimental error, and the repassivation potentials are almost identical. The breakdown potential associated with localized corrosion increased with Cu additions above 8 atom %, from −1020 mV SCE for 8 atom % Cu to −717 mV SCE for 27 atom % Cu (Fig. 12c-e). The cathodic loops and peaks associated with Zn back-plating are seen in the reverse scans. The results of the OCP and the breakdown potential of the eta phase as a function of Cu concentration in basic solutions are plotted in Fig. 15.

The polarization behavior of $Mg(Zn, Al)_2$ thin films in the high pH solution is shown in Fig. 16. The breakdown potential associated with localized corrosion does not vary significantly up to 10 atom % addition of aluminum (Fig. 17).

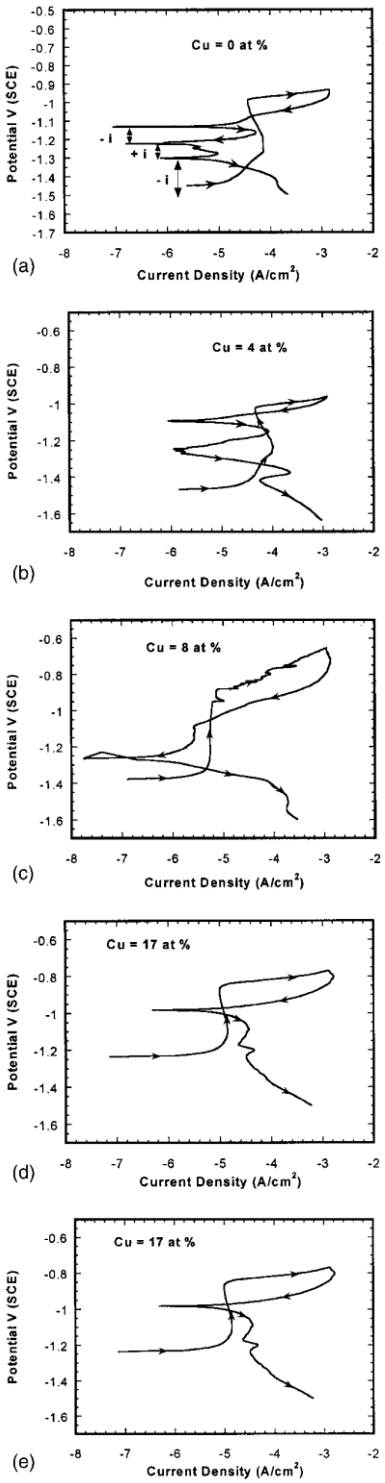

Figure 14. Polarization curve of $Mg(Zn, Cu)_2$ in deaerated 0.5 M NaCl (pH 10.94) at a scan rate of 5 mV/s. **(**a**)** Cu = 0 atom %, **(**b**)** Cu = 4 atom %, **(**c**)** Cu = 8 atom %, **(**d**)** Cu = 17 atom %, and **(**e**)** Cu = 27 atom %. Current polarity is indicated on the graphs in the reverse scan.

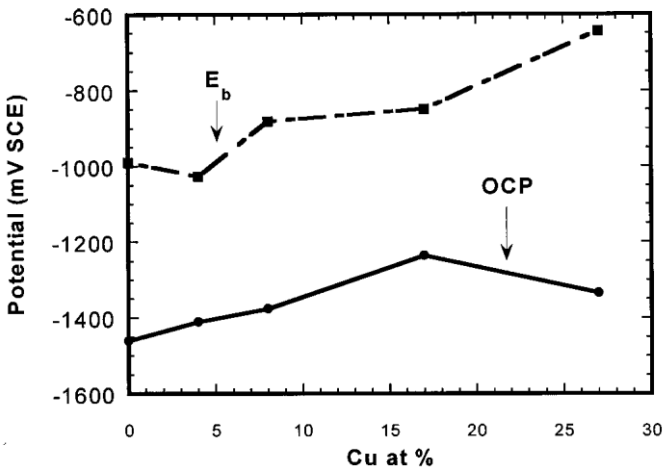

Figure 15. Variation in OCP and breakdown potential as a function of Cu concentration of $Mg(Zn, Cu)_2$ in deaerated 0.5 M NaCl (pH 10.94).

Effect of oxygen content in $Mg(Zn, Cu)_2$.—Oxygen contamination of the intermetallic thin films can have a large effect on the electrochemical behavior. Figure 18 shows the polarization curves in 0.5 M NaCl for two thin film samples with about the same Cu concentration. The film with the higher oxygen content (~3 atom %) had a higher OCP and breakdown potential compared to that with lower oxygen content (~1 atom%). It is important to realize that small quantities of oxygen can have a large influence on the electrochemical response of thin films.

Relevance to IGC of 7xxx series.—To summarize the results, electrochemical studies on the eta phase ($Mg(Zn, Cu)_2$ and $Mg(Zn, Al)_2$) as a function of Cu, Zn, and Al concentration in deaerated 0.5 M NaCl show that this phase is very active and has a breakdown potential that is associated with dealloying of Zn. In high pH solutions where $Mg(OH)_2$ is stable, the films are susceptible to amore classical form of localized breakdown. The breakdown potential increases with increasing copper concentration, but is relatively unaffected by Al addition. OCP playback experiments show that eta phase dissolves actively over a wide range of compositions in neutral aerated solutions at the OCP of AA7150.

The OCP and breakdown potentials of the eta phase thin films are well below the pitting potential of the 7xxx series alloys for the compositions studied. This suggests that the grain boundary intermetallic phases undergo preferential dissolution at potentials well below critical potentials associated with intergranular corrosion. In other words, the breakdown potentials seen in alloys such as AA7150 are well above the breakdown potential of the intermetallic phase and are thus not associated with the breakdown of these intermetallic phases.8 It is possible that the precipitate dissolution plays an indirect role in stabilizing IGC.8 This will be discussed in a future publication.

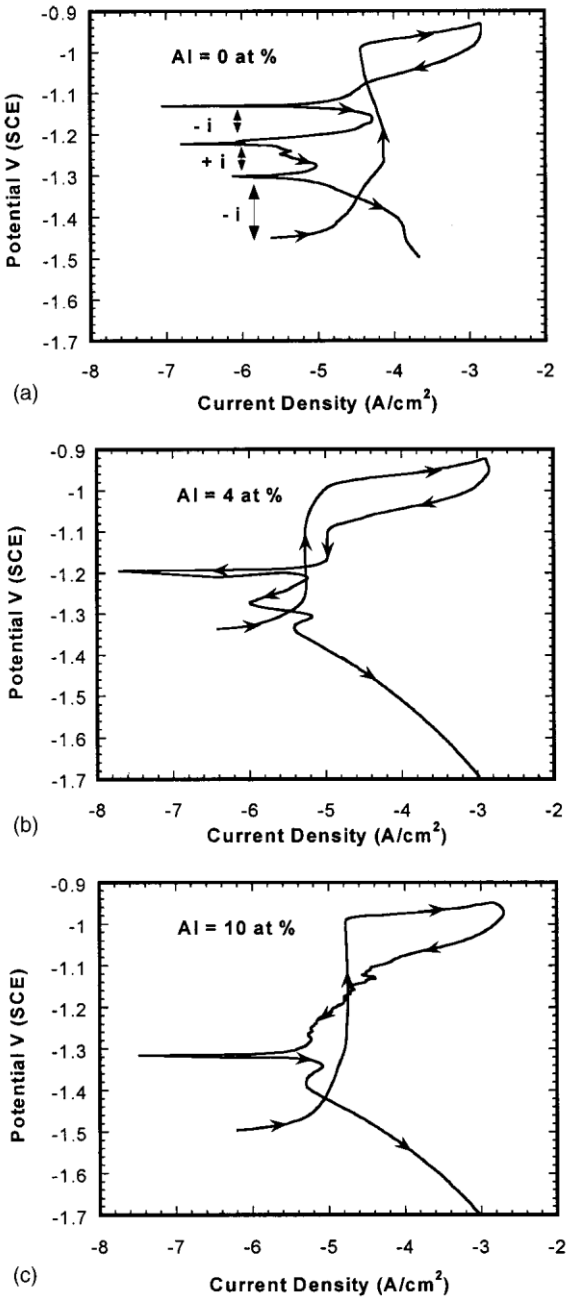

Figure 16. Polarization curve of $Mg(Zn, Al)_2$ in deaerated 0.5 M NaCl (pH 10.94) at a scan rate of 5 mV/s. **(**a**)** Al = 0 atom %, **(**b**)** Al = 4 atom %, and **(**c**)** Al = 10 atom %. Current polarity is indicated on the graphs in the reverse scan.

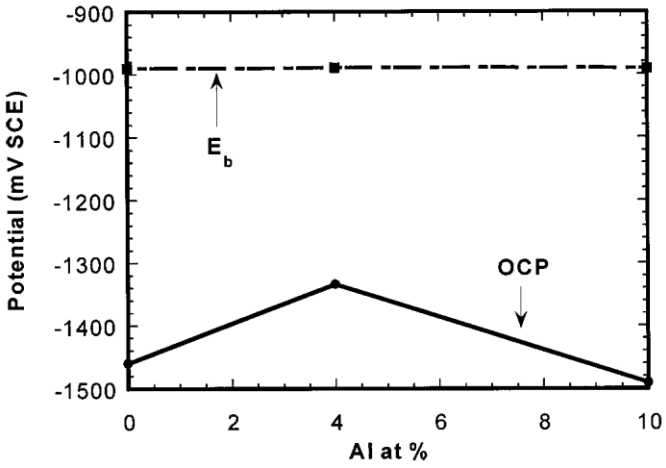

Figure 17. Variation in OCP and breakdown potential as a function of Al concentration of $Mg(Zn, Al)_2$ in deaerated 0.5 M NaCl (pH 10.94).

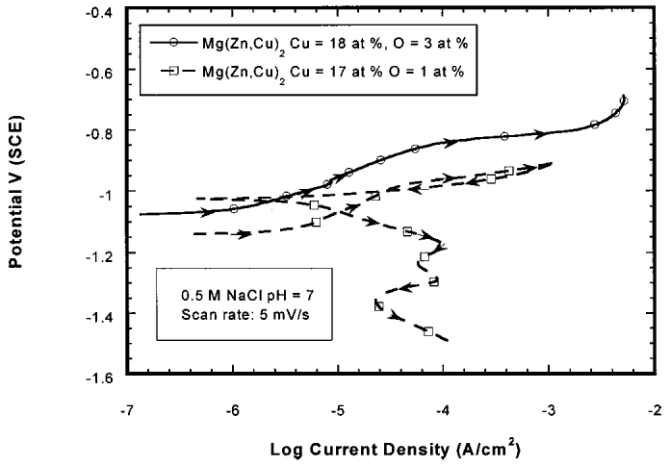

Figure 18. Polarization curves of $Mg(Zn, Cu)_2$ containing 18 atom % copper with differing oxygen content in deaerated 0.5 M NaCl at a scan rate of 5 mV/s.

Conclusions

Electrochemical tests were performed on intermetallic thin films of the eta phase in deaerated neutral and high pH 0.5 M NaCl. The following observations were made

1. $MgZn_2$ is very active and has an OCP of −1400 mV SCE in neutral 0.5 M NaCl, and a breakdown potential of −1140 mV SCE, which is associated with dealloying of Zn. Addition of up to 8 atom % Cu does not alter the breakdown potential of $MgZn_2$, however additions of 17 and 27 atom % results in raising the corrosion potential by 250 and 300 mV, respectively. The breakdown potentials associated with dealloying were raised by 150 and 210 mV, respectively. However, the addition of up to 10 atom % Al does not alter the behavior of $MgZn_2$ significantly.

2. Cyclic polarization curves on the intermetallic thin films show a cathodic loop or peak in the cathodic scan, which is associated with Zn reduction.

3. The eta phase thin films in high pH solutions are susceptible to localized breakdown

due to the protection offered by the stability of $Mg(OH)_2$. The addition of Cu to $MgZn_2$ results in raising the breakdown potentials. The addition of up to 10 atom % Al does not alter the breakdown potential.

4. OCP playback experiments provide a unique way of studying the electrochemical response of bulk analogs of second phase intermetallic compounds at the OCP of the aluminum alloy. $Mg(Zn, Cu, Al)_2$ is active to the matrix in the 7xxx series alloys, over a wide range of compositions in neutral chloride solutions.

5. Small levels of oxygen incorporated into the thin films can result in significant increase in the corrosion and breakdown potential.

Acknowledgments

This work was supported by the United States Air Force Office of Scientific Research grant no. F49620-99-1-0103 under the guidance of Dr. Paul Trulove and by the Air Force Research Laboratory under the guidance of Dr. Kumar Jata, contract F33615-96-D-5835.

Ohio State University assisted in meeting the publishing costs of this article.

References

1. R. G. Buchheit, *J. Electrochem. Soc.*, **142**, 3994 (1995).
2. R. Leard and R. G. Buchheit, The Ohio State University, Unpublished results.
3. J. R. Scully, T. O. Knight, R. G. Buchheit, and D. E. Pelebles, *Corros. Sci*., **33**, 185 (1993).
4. P. Schmutz and G. S. Frankel, *J. Electrochem. Soc*., **145**, 2285 (1998).
5. R. G. Buchheit, L. P. Montes, M. A. Martinez, J. Michael, and P. F. Hlava, *J. Electrochem. Soc*., **146**, 4424 (1999).
6. R. G. Buchheit, M. A. Martinez, and L. P. Montes, *J. Electrochem. Soc*., **147**, 119 (2000).
7. B. W. Lifka, D. O. Sprowls, and J. G. Kaufman, *Corrosion*, **23**, 335 (1967).
8. T. Ramgopal and G. S. Frankel, Unpublished results.
9. S. Maitra and G. C. English, *Metall. Trans. A*, **12**, 535 (1981).
10. E. Mattson, L. O. Gullman, L. Knotsson, R. Sundberg, and B. Thundal, *Br. Corros. J.*, **6**, 73 (1971).
11. A. J. Sedriks, J. A. S. Green, and D. L. Novak, *Localized Corrosion*, R. W. Staehle, B. F. Brown, J. Kruger, and A. Agarwal, Editors, NACE Houston, TX (1971).
12. L. I. Maissel and R. Glang, Editors, *Handbook of Thin Film Technology*, McGraw-Hill, New York (1970).
13. G. S. Frankel, J. R. Scully, and C. V. Jahnes, *J. Electrochem. Soc.*, **143**, 1834 (1996).
14. R. G. Buchheit, J. P. Moran, and G. E. Stoner, *Corrosion*, **46**, 610 (1990).
15. M. Pourbaix, *Atlas of Electrochemical Equilibria in Aqueous Solutions*, NACE, Houston, TX (1974).
16. G. S. Frankel, R. C. Newman, C. V. Jahnes, and M. A. Russak, *J. Electrochem. Soc*., **140**, 2192 (1993).